Clinical Spectroscopy 3 (2021) 100017

Contents lists available at ScienceDirect

Clinical Spectroscopy

journal homepage: www.sciencedirect.com/journal/clinical-spectroscopy

"A spectroscopic picture paints 1000 words" mapping iron speciation in brain tissue with "full spectrum per pixel" X-ray absorption near-edge structure spectroscopy

Mark J. Hackett [a,b,*], Gaewyn Ellison [a,b], Ashley Hollings [a,b], Frederick Colbourne [c], Martin D. de Jonge [d], Daryl L. Howard [d]

[a] School of Molecular and Life Sciences, Curtin University, Perth, WA 6845, Australia
[b] Curtin Health Innovation Research Institute, Curtin University, Perth, WA 6102, Australia
[c] Department of Psychology, University of Alberta, Edmonton, AB 26G2R3, Canada
[d] Australian Synchrotron, ANSTO Melbourne, 800 Blackburn Road, Clayton, VIC 3168, Australia

ARTICLE INFO

Keywords:
Coordination chemistry
Chemically specific imaging
XANES
Bioinorganic chemistry
Analytical spectrometry

ABSTRACT

Coordination chemistry enables a variety of vital functions in biological systems; however, characterising the chemical form of metal ions in cells and tissue is notoriously difficult. One technique that is gaining substantial momentum in this research area is X-ray absorption near-edge structure (XANES) spectroscopy. The XANES spectrum can be a rich source of information with respect to the coordination environment of metal ions. Further, XANES spectroscopy is compatible with microscopy mapping protocols as the spectra are recorded across a relatively narrow range of data points (typically 50–100). Although the potential of XANES spectroscopy to study metal ion coordination chemistry has long been known, data collection speed has only relatively recently reached the state in which maps can be collected with a full spectrum per pixel. The realisation of this capability now places XANES spectroscopic mapping among a suite of other spectroscopic imaging techniques, such as Fourier transform infrared (FTIR) spectroscopy and Raman spectroscopy, which are available to characterise biochemical composition, in situ within cells and tissue. Herein, we report a proof-of-concept application of XANES spectroscopic mapping to begin exploration of Fe speciation in brain tissue, which demonstrates the potential of this method for the biomedical sciences, and identifies important areas for consideration with respect to future protocol developments.

1. Introduction

The development of faster detection systems and higher spatial resolution imaging has thrust various modalities of spectroscopy (e.g., vibrational spectroscopy) beyond fundamental research and into the clinical laboratory [1–3]. Aside from vibrational spectroscopy however, there exists a host of other spectroscopic methods that show strong potential to illuminate the underlying biological chemistry of cells and tissues. One such technique is X-ray absorption near-edge structure spectroscopy (XANES spectroscopy). XANES spectroscopy measures the excitation of core electrons to unoccupied molecular orbitals, which inherently renders the technique highly sensitive to oxidation state and coordination environment (e.g., coordination geometry and ligand type) [4–16]. XANES has long been used to study the structure of biologically important metal ion coordination complexes [5,6], but the technique has only recently found applications as an imaging tool [9,10,17–19]. Critical improvements in the speed of XANES data collection have been achieved through improved detector efficiencies, improved detection electronics, and improved X-ray focussing optics, which when coupled with bright X-ray sources, now make XANES spectroscopic imaging, with a full XANES spectrum per pixel, a reality for the biological sciences [9,10,17,20–22].

In many ways, the current trajectory of biological applications of XANES spectroscopic mapping mirrors the path previously taken by techniques such as Fourier transform infrared (FTIR) spectroscopy and Raman spectroscopy. With increased advancements in instrumentation expected to lead to further accessibility to XANES spectroscopic imaging (e.g., lab based coherent X-ray sources) [23], future applications of

* Corresponding author at: School of Molecular and Life Sciences, Curtin University, Perth, WA 6845, Australia.
E-mail address: mark.j.hackett@curtin.edu.au (M.J. Hackett).

https://doi.org/10.1016/j.clispe.2021.100017
Received 15 June 2021; Accepted 11 October 2021
Available online 14 October 2021

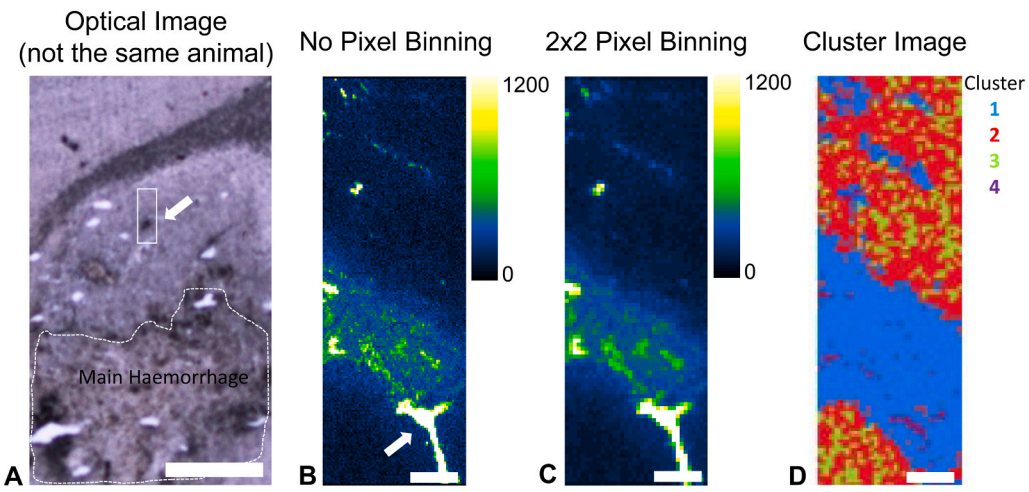

Fig. 1. XANES spectroscopic mapping reveals differences in brain-iron speciation after intracerebral haemorrhage. (A) An optical image of a tissue sample similar to that analysed in this study (but from a different animal), shows the ability to visualise haemorrhage by tissue discolouration due to bleeding. The main haemorrhage is outlined by a dashed white line, and a smaller haemorrhage (similar to that analysed in this study) is indicated by white box and white arrow. (B) Elemental map of total Fe distribution collected with a 2×2 μm pixel size, and then (C) the same map after 2×2 pixel binning to yield a 4×4 μm pixel size. (D) Each pixel in the map in C, contains an Fe XANES spectrum, which was processed with K-means clustering (following PCA data reduction) to yield a 4 cluster image. Scale bar in A = 500 μm, scale bar in B-D = 50 μm.

XANES spectroscopy in a clinical or diagnostic context may be realised. With this in mind, and in the context of this special issue (Biomedical Imaging), this article aims to showcase the potential of XANES spectroscopic mapping to study metal ion speciation in situ in biological samples, specifically with a case study of Fe speciation in rodent brain tissue.

In this proof-of-concept study we highlight two applications of XANES spectroscopic mapping to study Fe speciation in brain tissue: (1) we analyse Fe speciation following haemorrhagic stroke in the rat, and (2) we analyse Fe speciation within hippocampal neurons and the surrounding white matter tissue in a senescent mouse brain. In both cases, the XANES spectra show variation that indicate the presence of multiple chemical forms of Fe, which are found to co-localise with different anatomical features of the brain. A unique aspect to the data presented in this article, is that the data sets contain a full XANES spectrum per pixel, as opposed to most previous approaches where only a handful of representative XANES spectra are collected. It is our understanding that this study is the first report of "full XANES spectrum per pixel" mapping of brain tissue, at the Fe K-edge. We wish to emphasise that the results presented are not intended to reflect an exhaustive characterisation of the data, nor to present a fully validated XANES mapping protocol. Rather, the intent of this study is to demonstrate the future potential of XANES spectroscopic mapping for the biomedical communities, and to highlight similarities between XANES spectroscopy and other commonly used biospectroscopic imaging methods (such as vibrational spectroscopy).

2. Methods

2.1. Animal model and sample preparation

Two samples were prepared and analysed in this study, one sample was prepared from rat brain tissue after intracerebral haemorrhage, the other sample from a naturally aged wildtype mouse. Intracerebral haemorrhage was induced in a young-adult Sprague-Dawley rat by striatal collagenase injection as previously described [24,25]. All protocols in this study followed Canadian Council of Animal Care Guidelines and were approved by the Biosciences Animal Care and Use Committee at the University of Alberta. Tissue prepared from the senescent mouse brain (female C57BL/6 J, 24 months) was excess tissue from a dedicated study on the effect of ageing on brain inflammation (approved by Curtin University animal ethics committee). Both rat and mouse were humanely sacrificed under isoflurane anaesthetic, the brain tissue rapidly obtained and flash frozen in liquid nitrogen. A 20-μm-thick tissue section (rat) and a 10-μm-thick tissue section (mouse) were cut using a cryo-microtome and air-dried onto a 1-μm thick silicon nitride window manufactured by Silson, Canada (rat tissue) or the Melbourne centre for nano-fabrication (mouse tissue).

2.2. XANES mapping data collection

XANES-spectroscopic maps were collected at the X-ray Fluorescence Microscopy beamline at the Australian Synchrotron [15,26], using a "XANES-stack", which are a series of X-ray fluorescence elemental maps collected from the same sample area, but across a series of incremental incident X-ray energies. In this study the Fe K-edge XANES-spectroscopic maps were collected from 7080 to 7200 eV (rat brain), or 7100–7160 eV (mouse brain). An energy step size of 0.5 eV was used across the white line features, 7100–7160 eV, for both tissue samples. The XANES spectra were calibrated to 7112 eV for the first inflection point of elemental Fe. Both the XANES spectral maps were collected with a 2 ms dwell and 2 μm steps using a motorised sample stage, and a micro-focussed X-ray beam – focussed to a spot size of 2 μm (2-σ) using a Kirkpatrick–Baez mirror pair. The method used in this study is similar to those previously described in the literature [8–10,17]. X-ray fluorescence emission from the sample was recorded in back scatter geometry (sample orientated normal to the incident beam), using event-mode, by the low-latency, 384-pixel Maia detector [21]. Elemental maps were reconstructed from the full emission spectra with GeoPIXE v6.6j (CSIRO, Australia), as in our previous studies [27–29].

2.3. XANES mapping data analysis

Elemental maps of Fe fluorescence intensity were extracted as TIFF files from GeoPIXE, which were then imported into ImageJ v1.48 and converted into a Z-stack (Z-dimension equating to incident energy). To improve spectral signal to noise 2×2 pixel binning was applied, to yield images with a 4×4 μm pixel size. Fe-XANES spectra were normalised to a uniform Fe content to enhance sensitivity to differences in the chemical form of Fe, rather than just net differences in total Fe amount. To normalise the XANES spectra, the Z-stack was divided by the Fe elemental map collected above the K-edge (7180 eV for rat brain sample, 7160 eV for mouse brain sample). The normalised Z-stack was then exported from ImageJ and imported into Mantis 2.3.02, where principle component analysis (PCA) was applied across the full spectrum for data reduction, subsequent to K-means cluster analysis (a 4 group cluster

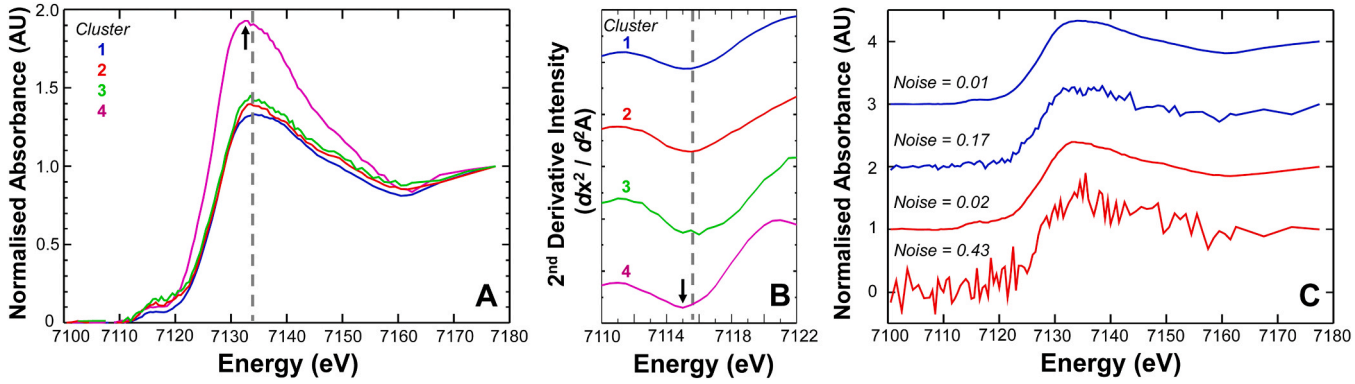

Fig. 2. Average XANES spectra of the 4 clusters presented in Fig. 1D. (A) A characteristic broadening of the white line features associated with haemoglobin can be seen in cluster1 (blue trace), while cluster 4 (purple trace) contains markedly increased white line intensity that is shifted to a lower energy (indicated by dashed line and black arrow). (B) The shift in white line position observed for cluster 4 (panel A), is also reflected in the second-derivatives of the pre-edge feature (1 s – 3d), as shown by dashed line and black arrow. (C) Assessment of noise in average XANES spectra of cluster 1 (blue) and 2 (red), in addition to representative single-pixel XANES spectra from cluster 1 and 2 presented beneath each cluster average. (For interpretation of the references to colour in this figure legend, the reader is referred to the web version of this article.)

analysis was applied for both samples). The average XANES spectra from each cluster, as well as representative single-pixel XANES spectra were further analysed using the EXAFPAK suite of data analysis programs [30].

3. Results

3.1. Analysis of Fe speciation within and around brain-haemorrhages

XANES spectroscopic mapping was applied to a coronal cross section of rat brain tissue, from an animal model of intra-cerebral haemorrhage (Fig. 1A-D). In this animal model, the site of haemorrhage and bleeding can be identified with optical microscopy in unstained tissue, through visualisation of the blood [24]. Unfortunately, an optical image was not recorded for the exact sample analysed with XANES spectroscopic imaging in this study. However, an optical image from one of our previous published studies using this model is presented in Fig. 1A [24], to highlight how the optical image can be used to identify the location of a haemorrhage. For this current study we aimed to image a range of different chemical forms of Fe in brain tissue (not just Fe from the blood), and therefore we chose not to image the main site of brain haemorrhage, but rather a smaller isolated bleed adjacent to the main haemorrhage was imaged (as shown in Fig. 1A).

The map of total Fe distribution (Fig. 1B) shows a band of elevated Fe content, which most likely corresponds to haemorrhaged tissue (although we cannot confirm with complete certainty). Within the band of elevated Fe, there exists a region of highly concentrated Fe (white arrow Fig. 1B), which is most likely a blood vessel (again, we cannot confirm with complete certainty). The elemental maps of total Fe distribution, 2×2 μm pixel and 4×4 μm pixel size are presented in Fig. 1B and C, respectively. Cluster analysis was applied to the normalised XANES spectral data set to produce 4 spectral clusters. The 4 cluster image is presented in Fig. 1D. The cluster image reveals two clusters within the proposed site of brain haemorrhage, while the surrounding brain tissue (low Fe regions) can also be grouped into two clusters.

The average spectra from each cluster highlight the potential of XANES spectroscopy to resolve and differentiate between different chemical forms of Fe in brain tissue. As this was a proof-of-concept study, XANES mapping was not undertaken in combination with the development of a spectral library of Fe model compounds or standard solutions. The published literature does however, contain numerous examples of Fe K-edge XANES spectra for relevant Fe compounds, which are expected to be abundant in the brain (e.g., haemoglobin, ferritin, ferrous and ferric iron complexes with organic acids), which enables simple visual comparison between the data in this study and the published literature. Differences between ferritin and haemoglobin XANES spectra have previously been well characterised, and specifically haemoglobin contains a less pronounced, broadened white line (1s–4p transition), with reduced intensity relative to the narrower more intense ferritin white line. Visual inspection of the XANES spectra for each cluster average (Fig. 2A) indicates spectral features consistent with haemoglobin in cluster 1 (max normalised white line intensity is 1.33 at 7133.8 eV), while the average spectra of clusters 2 and 3 are consistent with Ferritin (maximum white line intensity is 1.41 and 1.43, respectively, both at 7133.5 eV). The occurrence of maximum white line intensity across 7133–7134 eV in clusters 1–3, is consistent with predominantly ferric iron [31–34]. In contrast to clusters 1–3, the average spectra of cluster 4 displays a pronounced white line intensity (1.91), with the maxima shifted to lower energy (7131.4 eV). This shift to lower energy is consistent with increased abundance of ferrous iron. This shift of the white line to lower energy for the average spectra of cluster 4, matches well with a shift to lower energy of the pre-edge feature (1s – 3d transition) [33], as observed in the second-derivative spectra. Specifically, in the second-derivative minima of the pre-edge feature for cluster 4 occurs at 7114.9 eV, while clusters 1–3 occur at 7115.4 eV (Fig. 2B). The large increase in white line intensity that is observed for the average spectra of cluster 4 (e.g. normalised intensity of 1.91 compared to ~1.4 in other spectra) is indicative of increased local symmetry at the coordination site, and is reminiscent of published spectra of ferrous iron coordinated to organic acids, such as lactate and citrate [32,35].

The spectral signal to noise ratio (S/N) is an important consideration for interpreting XANES spectral images (indeed it is a critical consideration for all spectroscopic imaging), and S/N guides the choice of appropriate forms of data pre-processing (e.g., pixel binning, filtering) [36], or methods for image generation (e.g., linear fitting, principle component analysis, cluster analysis). To assist in future studies, we report the noise levels (calculated at the main white line feature) for average cluster spectra, and representative single spectra, as shown in Fig. 2C.

3.2. XANES-spectroscopic mapping analysis of Fe speciation within hippocampal pyramidal neurons (grey matter), and the adjacent corpus callosum white matter

XANES spectroscopic imaging was applied across a coronal section of a mouse hippocampus (wildtype C57B/6, age 24 months). The region of

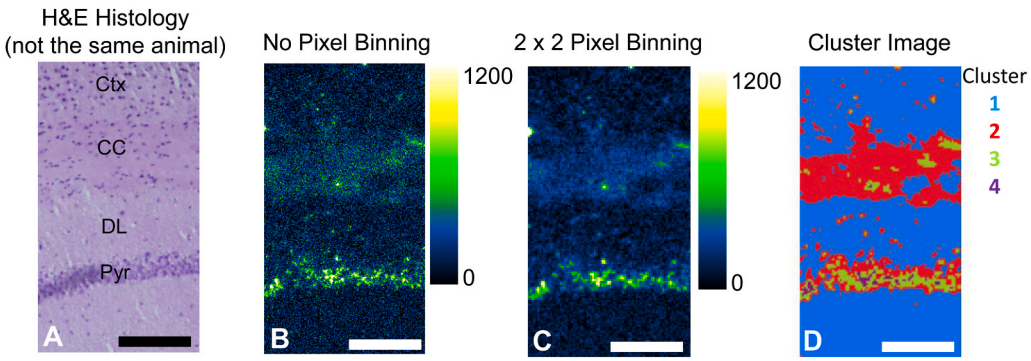

Fig. 3. XANES spectroscopic mapping reveals differences in brain-iron speciation in the senescent mouse hippocampus. (A) An optical image of H&E stained mouse hippocampus tissue (a different mouse than what was analysed in this study). The H&E image shows an equivalent region to that analysed in this study, and the major anatomic regions are annotated. Ctx = cortical layers, CC = corpus callosum white matter, DL = hippocampus dendritic layers, Pyr = Hippocampal pyramidal neuron layer. (B) Elemental map of total Fe distribution collected with a 2 × 2 μm pixel size, and then (C) the same map after 2 × 2 pixel binning to yield a 4 × 4 μm pixel size. (D) Each pixel in the map in C, contains an Fe XANES spectrum, which was processed with K-means clustering (following PCA data reduction) to yield a 4 cluster image. Scale bars in A - D = 100 μm.

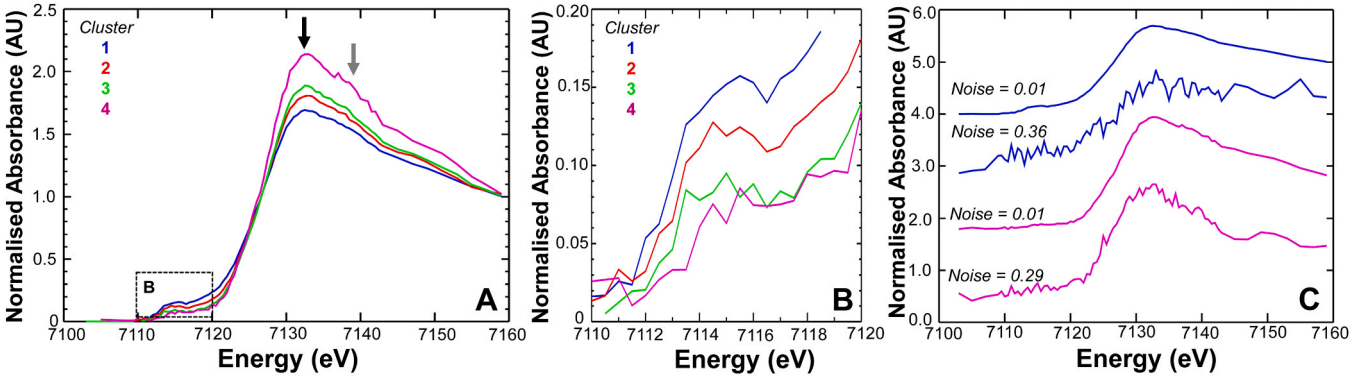

Fig. 4. Average XANES spectra of the 4 clusters presented in Fig. 2D. (A) Subtle differences in intensity are observed the average XANES spectra of clusters 1–3, however a marked increase in white line intensity is observed for the spectra of cluster 4 (black arrow). In addition, a pronounced high energy shoulder is observed for cluster 4 (grey arrow), but a much weaker pre-edge feature (1s – 3d transition) is seen (black box). (B) A close-up view of the pre-edge region shown in the block box in A, highlighting the weaker pre-edge intensity of cluster 4. (C) Assessment of noise in average XANES spectra of cluster 1 and 4, in addition to representative single-pixel XANES spectra from cluster 1 and 4.

tissue analysed contains 4 major tissue types, the hippocampal pyramidal neuron cell layer (grey matter, enriched with cell bodies and nuclei of neurons), hippocampal dendritic layers (some cell bodies, but mainly neuron dendrites, and supporting cells such as glia), the corpus callosum white matter (enriched in myelinated axons), and cortex (scattered neuron cell bodies and dendrites). These regions are annotated on the H&E histology shown in Fig. 3A. The total Fe elemental maps for 2 × 2 μm, and 4 × 4 μm pixel sizes are presented in Fig. 3B and C, respectively. Cluster analysis was applied to the XANES spectra, and the 4 cluster image is presented in Fig. 3D. In general, spectra from the hippocampal dendritic layers and cortex cluster together. A second cluster is found to colocalise to the corpus callosum white matter, and the outside margins of the hippocampal pyramidal neuron cell layer. Within the pyramidal neuronal cell layer, 2 clusters are observed. We have previously shown that pyramidal neurons are enriched in Fe, and indeed this study shows the characteristic punctate Fe distribution in the neuronal cell layer, similar to our previous study (Fig. 3D) [27]. The average XANES spectrum of cluster 1 (hippocampal dendritic layers, and corpus callosum) visibly resembles that of ferritin, published throughout the literature [9,37], (normalised white line intensity 1.69 at 7133 eV, Fig. 3D). The average spectra for clusters 2 and 3 are similar to that of cluster 1, but with subtle changes in the intensity and position of the white line (cluster 2: normalised white line intensity of 1.81 at 7133 eV, cluster 3: normalised white line intensity of 1.88 at 7132.5 eV). These subtle changes in white line intensity and position suggest variation in one or several chemical forms of Fe contributing to the average spectrum. The most pronounced spectroscopic difference observed in the mouse hippocampus is the average XANES spectra for cluster 4, which colocalises with the regions of most intense Fe content within the hippocampal pyramidal neuron cell layer. The average XANES spectrum of cluster 4 shows increased white line intensity (normalised intensity of 2.15 at 7132.5 eV), and a pronounced high energy shoulder (white arrow, 4A). Despite the increased white line intensity, the average spectrum of cluster 4 shows a noticeably reduced intensity of the pre-edge feature (1 s – 3d transition), as shown in Fig. 4B. Exact identification of the underlying chemical forms of Fe responsible for these changes is not possible at this time, however increased white line intensity and reduced pre-edge intensity is characteristic of an octahedral coordination environment. Further, the high energy shoulder observed on the white line may indicated coordination with phosphates [37].

A comparison of spectral signal to noise was undertaken for the mouse brain tissue section, as described for the rat brain tissue. As would be expected, noise levels are substantially higher (~30x) in the single pixel spectrum compared to the cluster averages, as shown in Fig. 4C.

4. Discussion

The results of this study highlight the unique opportunities that are available to characterise Fe speciation in brain tissue, when data is collected with a full XANES spectrum per pixel. This study however, also reveals that in-depth data-exploration and analysis strategies need to be developed to take advantage of the richness of information contained

within the data set. Based on the published literature, a pronounced difference in the Fe K-edge XANES spectrum would be expected for tissue locations enriched in haemoglobin, and indeed this was observed at the site of haemorrhage in the rat brain tissue analysed in this study. Interestingly, the majority of spectra from the other cluster averages, for both rat and mouse bran tissue, visually resemble ferritin. Upon closer inspection and detailed analysis of the normalised edge position and intensity, there are numerous subtle differences between the spectra, which differ from those reported for ferritin in the literature. These subtle differences in both the normalised intensity of the white line, position of the white line, and shoulders or broadenings of the white line features point to a diverse array of Fe chemical species contributing to the average spectrum. On the basis of the results in this study it is clear that a detailed spectral library, which models the different coordination environments of Fe that are expected to be found in brain tissue, is required.

The shifts in the position of the white line observed in this study possibly indicate variation in Fe oxidation state across different tissue structures (not unexpected). Indeed, the application of XANES spectroscopic imaging to investigate Fe oxidation state is already of immense research interest [10], especially with respect to studying relationships between brain-Fe accumulation and oxidative stress during natural ageing or neurodegenerative disease. However, it is well established that shifts in the position of XANES spectral features arise from not only changes in oxidation state, but also the type of coordinating ligand, the ligand coordination geometry, and the spin state of the metal ion. As an example, a great diversity in XANES spectral features has been shown for a range of biologically relevant Zn complexes or standard solutions [4,8,11], which all exist in the same oxidation state. Unfortunately, the sensitivity of the XANES spectrum to multiple facets of the underlying metal ion coordination environment complicates interpretation of the data; however, it also provides an avenue for detailed insight of metal ion coordination chemistry in biological systems.

Sample preparation is an important consideration for spectroscopic chemical imaging, and detailed studies have been undertaken across the biospectroscopy community. In this study a spectroscopic signature that resembled Fe coordinated to phosphates was observed within the hippocampal pyramidal neuron layer. Recently it was observed that air-drying tissue sections drastically increases coordination of Zn through phosphate groups, which is not replicated when frozen tissues are analysed. This raises the question of the effect of air-drying on Fe speciation in brain tissue, and whether Fe – phosphate complexes are abundant in vivo, or if this observation is an artefact of sample preparation. It is therefore, imperative to now compare Fe XANES spectra collected from chemically fixed, air-dried, and frozen tissues (among other preparations) to fully characterise the effects sample preparation may have on Fe speciation. Lastly, given the known effect of photo-damage on both morphology, elemental distribution, and oxidation state of biological samples [38–42], it would be pertinent to undertake a detailed assessment of how radiation damage may impact Fe speciation in brain tissue.

5. Conclusions

To our knowledge, this is the first study to report XANES spectroscopic imaging of brain tissue at the Fe K-edge, with a full XANES spectrum recorded at each pixel in the image. This capability has enabled subsequent K-means cluster analysis, which demonstrated the ability to detect differences in the chemical form of Fe between different brain tissue structures (e.g., neuronal layer vs white matter) or as a consequence of pathology (e.g., haemorrhage). In itself the results are not especially surprising, but taken together with the trajectory of this research field, this study highlights the future potential of XANES spectroscopic imaging, when coupled with an appropriate spectroscopic library, to investigate Fe speciation in detail within brain tissue.

Declaration of Competing Interest

The authors declare that they have no known competing financial interests or personal relationships that could have appeared to influence the work reported in this paper.

Acknowledgements

MJH gratefully acknowledges current support from the Australian Research Council (ARC Future Fellowship FT190100017). MJH acknowledges past support from the Dementia Australia Research Foundation, Mamutil New Investigator Project Grant (11646), and past support from the Canadian Institute of Health Research (CIHR). AH acknowledges the support from the Australian Government through an Australian Government Research Training Program Scholarship and an Australian Institute of Nuclear Science and Engineering Post Graduate Research Award (AINSE-PGRA). Components of this research was supported by a Heart and Stroke Foundation of Canada/Canadian Institutes of Health Research Synchrotron Medical Imaging team grant to FC, and others. FC is a Canada Research Chair in Intracerebral Hemorrhagic Stroke. We gratefully acknowledge travel funding provided by ANSTO, funded by the Australian Government. This research was undertaken at the X-ray fluorescence microscopy (XFM) beamlines at the Australian Synchrotron, ANSTO, Victoria, Australia. This work was performed in part at the Melbourne Centre for Nanofabrication (MCN) in the Victorian Node of the Australian National Fabrication Facility (ANFF). The authors wish to acknowledge the assistance and expertise provide by Dr Connie Jackaman and Lelinh Duong for collection and provision of wildtype mouse brain tissue.

References

[1] D.C. Fernandez, R. Bhargava, S.M. Hewitt, I.W. Levin, Infrared spectroscopic imaging for histopathologic recognition, Nat. Biotechnol. 23 (4) (2005) 469–474.
[2] M.J. Baker, J. Trevisan, P. Bassan, R. Bhargava, H.J. Butler, K.M. Dorling, P. R. Fielden, S.W. Fogarty, N.J. Fullwood, K.A. Heys, C. Hughes, P. Lasch, P. L. Martin-Hirsch, B. Obinaju, G.D. Sockalingum, J. Sulé-Suso, R.J. Strong, M. J. Walsh, B.R. Wood, P. Gardner, F.L. Martin, Using Fourier transform IR spectroscopy to analyze biological materials, Nat. Protoc. 9 (8) (2014) 1771–1791.
[3] M.J. Baker, H.J. Byrne, J. Chalmers, P. Gardner, R. Goodacre, A. Henderson, S. G. Kazarian, F.L. Martin, J. Moger, N. Stone, Clinical applications of infrared and Raman spectroscopy: state of play and future challenges, Analyst 143 (8) (2018) 1735–1757.
[4] O. McCubbin Stepanic, J. Ward, J.E. Penner-Hahn, A. Deb, U. Bergmann, S. DeBeer, Probing a silent metal: a combined X-ray absorption and emission spectroscopic study of biologically relevant zinc complexes, Inorg. Chem. 59 (18) (2020) 13551–13560.
[5] J.E. Penner-Hahn, X-ray absorption spectroscopy in coordination chemistry, Coord. Chem. Rev. 190 (1999) 1101–1123.
[6] J.E. Penner-Hahn, Characterization of “spectroscopically quiet” metals in biology, Coord. Chem. Rev. 249 (1–2) (2005) 161–177.
[7] S.A. Wilson, E. Green, I.I. Mathews, M. Benfatto, K.O. Hodgson, B. Hedman, R. Sarangi, X-ray absorption spectroscopic investigation of the electronic structure differences in solution and crystalline oxyhemoglobin, Proc. Natl. Acad. Sci. USA 110 (41) (2013) 16333–16338.
[8] A.L. Hollings, V. Lam, R. Takechi, J.C. Mamo, J. Reinhardt, M.D. de Jonge, P. Kappen, M.J. Hackett, Revealing differences in the chemical form of zinc in brain tissue using K-edge X-ray absorption near-edge structure spectroscopy, Metallomics 12 (12) (2020) 2134–2144.
[9] S.A. James, D.J. Hare, N.L. Jenkins, M.D. de Jonge, A.I. Bush, G. McColl, φXANES: In vivo imaging of metal-protein coordination environments, Sci. Rep. 6 (2016) 20350.
[10] S.A. James, B.R. Roberts, D.J. Hare, M.D. de Jonge, I.E. Birchall, N.L. Jenkins, R. A. Cherny, A.I. Bush, G. McColl, Direct in vivo imaging of ferrous iron dyshomeostasis in ageing Caenorhabditis elegans, Chem. Sci. 6 (5) (2015) 2952–2962.
[11] S.A. Thomas, B. Mishra, S.C.B. Myneni, High energy resolution-X-ray absorption near edge structure spectroscopy reveals Zn ligation in whole cell bacteria, J. Phys. Chem. Lett. 10 (10) (2019) 2585–2592.
[12] A. Carmona, S. Roudeau, L. Perrin, C. Carcenac, D. Vantelon, M. Savasta, R. Ortega, Mapping chemical elements and iron oxidation states in the substantia nigra of 6-hydroxydopamine lesioned rats using correlative immunohistochemistry with proton and synchrotron micro-analysis, Front. Neurosci. 13 (2019) 1014.
[13] J. Chwiej, D. Adamek, M. Szczerbowska-Boruchowska, A. Krygowska-Wajs, S. Wojcik, G. Falkenberg, A. Manka, M. Lankosz, Investigations of differences in iron oxidation state inside single neurons from substantia nigra of Parkinson’s

disease and control patients using the micro-XANES technique, J. Biol. Inorg. Chem. 12 (2) (2007) 204–211.
[14] Y. Pushkar, G. Robison, B. Sullivan, S.X. Fu, M. Kohne, W. Jiang, S. Rohr, B. Lai, M. A. Marcus, T. Zakharova, Aging results in copper accumulations in glial fibrillary acidic protein-positive cells in the subventricular zone, Aging Cell 12 (5) (2013) 823–832.
[15] B. Sullivan, G. Robison, J. Osborn, M. Kay, P. Thompson, K. Davis, T. Zakharova, O. Antipova, Y. Pushkar, On the nature of the Cu-rich aggregates in brain astrocytes, Redox Biol. 11 (2017) 231–239.
[16] H. Wang, M. Wang, B. Wang, M. Li, H. Chen, X. Yu, Y. Zhao, W. Feng, Z. Chai, The distribution profile and oxidation states of biometals in APP transgenic mouse brain: dyshomeostasis with age and as a function of the development of Alzheimer's disease, Metallomics 4 (3) (2012) 289–296.
[17] S.A. James, R. Burke, D.L. Howard, K.M. Spiers, D.J. Paterson, S. Murphy, G. Ramm, R. Kirkham, C.G. Ryan, M.D. de Jonge, Visualising coordination chemistry: fluorescence X-ray absorption near edge structure tomography, Chem. Commun. 52 (79) (2016) 11834–11837.
[18] M.J. Pushie, I.J. Pickering, M. Korbas, M.J. Hackett, G.N. George, Elemental and chemically specific X-ray fluorescence imaging of biological systems, Chem. Rev. 114 (17) (2014) 8499–8541.
[19] M.J. Hackett, P.G. Paterson, I.J. Pickering, G.N. George, Imaging taurine in the central nervous system using chemically specific X-ray fluorescence imaging at the sulfur K-edge, Anal. Chem. 88 (2016) 10916–10924.
[20] L.A. Fisher, D. Fougerouse, J.S. Cleverley, C.G. Ryan, S. Micklethwaite, A. Halfpenny, R.M. Hough, M. Gee, D. Paterson, D.L. Howard, K. Spiers, Quantified, multi-scale X-ray fluorescence element mapping using the Maia detector array: application to mineral deposit studies, Mineralium Deposita 50 (6) (2015) 665–674.
[21] C. Ryan, D. Siddons, R. Kirkham, Z. Li, M. de Jonge, D. Paterson, A. Kuczewski, D. Howard, P. Dunn, G. Falkenberg, MAIA X-ray fluorescence imaging: capturing detail in complex natural samples, J. Phys.: Conf. Ser. 499 (1) (2014), 012002.
[22] D.L. Howard, M.D. de Jonge, N. Afshar, C.G. Ryan, R. Kirkham, J. Reinhardt, C. M. Kewish, J. McKinlay, A. Walsh, J. Divitcos, The XFM beamline at the Australian synchrotron, J. Synchrotron Rad. 27 (5) (2020) 1447–1458.
[23] P. Zimmermann, S. Peredkov, P.M. Abdala, S. DeBeer, M. Tromp, C. Müller, J. A. van Bokhoven, Modern X-ray spectroscopy: XAS and XES in the laboratory, Coord. Chem. Rev. 423 (2020), 213466.
[24] M.J. Hackett, M. DeSouza, S. Caine, B. Bewer, H. Nichol, P.G. Paterson, F. Colbourne, A new method to image heme-Fe, total Fe, and aggregated protein levels after intracerebral hemorrhage, ACS Chem. Neurosci. 6 (5) (2015) 761–770.
[25] M.R. Williamson, K. Dietrich, M.J. Hackett, S. Caine, C.A. Nadeau, J.R. Aziz, H. Nichol, P.G. Paterson, F. Colbourne, Rehabilitation augments hematoma clearance and attenuates oxidative injury and ion dyshomeostasis after brain hemorrhage, Stroke 48 (2016) 195–203.
[26] D. Paterson, M. De Jonge, D. Howard, W. Lewis, J. McKinlay, A. Starritt, M. Kusel, C. Ryan, R. Kirkham, G. Moorhead, The X-ray fluorescence microscopy beamline at the Australian synchrotron, AIP Conf. Proc. 1365 (1) (2011) 219–222.
[27] M.J. Hackett, A. Hollings, S. Caine, B.E. Bewer, M. Alaverdashvili, R. Takechi, J.C. L. Mamo, M.W.M. Jones, M.D. de Jonge, P.G. Paterson, I.J. Pickering, G.N. George, Elemental characterisation of the pyramidal neuron layer within the rat and mouse hippocampus, Metallomics 11 (2019) 151–165.
[28] B.R. Lins, J.M. Pushie, M. Jones, D.L. Howard, J.G. Howland, M.J. Hackett, Mapping alterations to the endogenous elemental distribution within the lateral ventricles and choroid plexus in brain disorders using X-ray fluorescence imaging, PLoS One 11 (6) (2016), e0158152.
[29] K.L. Summers, N. Fimognari, A. Hollings, M. Kiernan, V. Lam, R.J. Tidy, D. Paterson, M.J. Tobin, R. Takechi, G.N. George, I.J. Pickering, J.C. Mamo, H. H. Harris, M.J. Hackett, A multimodal spectroscopic imaging method to characterize the metal and macromolecular content of proteinaceous aggregates ("Amyloid Plaques"), Biochemistry 56 (32) (2017) 4107–4116.
[30] George, G.N.; Pickering, I.J., EXAFSPAK: A Suite of Computer Programs for Analysis of X-ray Absorption Spectra. ⟨http://ssrl.slac.stanford.edu/exafspak.html⟩ 1995.
[31] M. Szczerbowska-Boruchowska, M. Lankosz, M. Czyzycki, D. Adamek, An integrated experimental and analytical approach to the chemical state imaging of iron in brain gliomas using X-ray absorption near edge structure spectroscopy, Anal. Chim. Acta 699 (2) (2011) 153–160.
[32] L. Grillet, L. Ouerdane, P. Flis, M.T.T. Hoang, M.-P. Isaure, R. Lobinski, C. Curie, S. Mari, Ascorbate efflux as a new strategy for iron reduction and transport in plants, J. Biol. Chem. 289 (5) (2014) 2515–2525.
[33] A.J. Berry, H.S.C. O'Neill, K.D. Jayasuriya, S.J. Campbell, G.J. Foran, XANES calibrations for the oxidation state of iron in a silicate glass, Am. Miner. 88 (7) (2003) 967–977.
[34] A. Al-Ebraheem, J. Goettlicher, K. Geraki, S. Ralph, M.J. Farquharson, The determination of zinc, copper and iron oxidation state in invasive ductal carcinoma of breast tissue and normal surrounding tissue using XANES, X-Ray Spectrom. 39 (5) (2010) 332–337.
[35] T. Rennert, K. Eusterhues, V. De Andrade, K.U. Totsche, Iron species in soils on a mofette site studied by Fe K-edge X-ray absorption near-edge spectroscopy, Chem. Geol. 332–333 (2012) 116–123.
[36] D. Hartnell, A. Hollings, A.M. Ranieri, H.B. Lamichhane, T. Becker, N.J. Sylvain, H. Hou, M.J. Pushie, E. Watkin, K.R. Bambery, M.J. Tobin, M.E. Kelly, M. Massi, J. Vongsvivut, M.J. Hackett, Mapping sub-cellular protein aggregates and lipid inclusions using synchrotron ATR-FTIR microspectroscopy, Analyst 146 (11) (2021) 3516–3525.
[37] A.N. Mansour, C. Thompson, E.C. Theil, N.D. Chasteen, D.E. Sayers, Fe(III).ATP complexes. Models for ferritin and other polynuclear iron complexes with phosphate, J. Biol. Chem. 260 (13) (1985) 7975–7979.
[38] G.N. George, I.J. Pickering, M.J. Pushie, K. Nienaber, M.J. Hackett, I. Ascone, B. Hedman, K.O. Hodgson, J.B. Aitken, A. Levina, X-ray-induced photo-chemistry and X-ray absorption spectroscopy of biological samples, J. Synchrotron Radiat. 19 (6) (2012) 875–886.
[39] Q. Xiao, A. Maclennan, Y. Hu, M. Hackett, P. Leinweber, T.-K. Sham, Medium-energy microprobe station at the SXRMB of the CLS, J. Synchrotron Radiat. 24 (1) (2017) 333–337.
[40] M.W.M. Jones, D.J. Hare, S.A. James, M.D. de Jonge, G. McColl, Radiation dose limits for bioanalytical X-ray fluorescence microscopy, Anal. Chem. 89 (22) (2017) 12168–12175.
[41] S. Lafuerza, M. Retegan, B. Detlefs, R. Chatterjee, V. Yachandra, J. Yano, P. Glatzel, New reflections on hard X-ray photon-in/photon-out spectroscopy, Nanoscale 12 (30) (2020) 16270–16284.
[42] M. Van Schooneveld, S. DeBeer, A close look at dose: toward L-edge XAS spectral uniformity, dose quantification and prediction of metal ion photoreduction, J. Electron. Spectrosc. Relat. Phenom. 198 (2015) 31–56.